# Spontaneous Oscillations in Hodgkin-Huxley Model

Tzyy-Leng Horng * Ming-Wai Huang

*Department of Applied Mathematics, Feng Chia University, Taichung, Taiwan, 407 ROC*

Received 26 July 2006; Accepted 24 Aug 2006

**Abstract**

Automatic neuron firing is an important and interesting research subject in neuroelectrophysiology. Through the original Hodgkin-Huxley model, we investigate its codimension 1 bifurcations along maximum conductance of the sodium channel, maximum conductance of potassium channel, and extracellular potassium concentration. We find that increasing maximum conductance of sodium channel, or decreasing maximum conductance of potassium channel, or increasing extracellular potassium concentration will all cause spontaneous oscillation without any external stimulus current. The effect of increasing extracellular potassium concentration will cause repetitive neuron firing has been verified by experiments, but the effect that changing maximum channel conductance will cause automatic neuron firing is first analyzed in the current paper but not yet verified by experiments. We hope the experiment can be done in the future by using sodium channel activator and potassium channel blocker.

***Keywords***: Hodgkin-Huxley model, Bifurcation analysis, Sodium channel, Potassium channel, Extracellular potassium concentration

## Introduction

The Hodgkin-Huxley model was first derived from the experiment with axon of the squid in 1952 [1]. The huge success of the Hodgkin-Huxley model drew broad attention and since then intensive researches have been conducted to study cell membrane action potential caused by the activity of all kinds of ionic channels in excitable cells such as neurons and cardiac cells. Among these researches, many are about the bifurcation study of parameters in models, and spontaneous oscillation is a major focus in this subject. The earliest bifurcation analysis was on external stimulus current *I*. When increasing *I*, the stable equilibrium point (resting potential state) will go through a subcritical Hopf bifurcation and become unstable. At the same time, the only attractor left is a stable limit cycle characterized by its spontaneous oscillation in time. Further increasing *I*, this stable limit cycle will go through a supercritical Hopf bifurcation and the oscillation disappears. Simultaneously, the previous unstable equilibrium point becomes stable again and the resting potential state once more dominates the whole dynamic [2-6].

Some other bifurcation analyses are about temperature [3, 7-9]. FitzHugh [7] studied the effect of temperature on action potential of squid axon and modified the original Hodgkin-Huxley equations by a temperature factor. Guttman and Barnhill [8] followed FitzHugh's work and found repetitive firing when increasing temperature by both experiment and computation. They also found that the firing frequency increases as the temperature increases. Feudel el al. [9] studied global bifurcations of the chaotic attractor in a modified Hodgkin–Huxley model of thermally sensitive neurons with temperature being the bifurcation parameter, and found a period-doubling cascade to chaos.

Bifurcation along with extracellular potassium concentration has also been intensively investigated. Aihara and Matsumoto [10] studied the bifurcation of slightly modified Hodgkin-Huxley equations along extracellular potassium concentration with and without constant external stimulus current, $I$ = 0 and $I = -20\mu A/cm^2$. They found, when $I$=0, the dynamics is first dominated by a stable equilibrium point (resting potential state) initially. When increasing extracellular potassium concentration, the dominant attractor becomes a stable limit cycle through a subcritical Hopf bifurcation and spontaneous oscillation occurs. When the concentration is further increased, the dynamics will again be dominated by a stable equilibrium point through a supercritical Hopf bifurcation and automatic neuron firing disappears. However, for $I = -20\mu A/cm^2$, they found bi-stability along the bifurcation of extracellular potassium concentration. The dynamics are first dominated by a stable equilibrium point and then changes to be dominated by a stable equilibrium point and limit cycle as extracellular potassium concentration is increased. Further increasing extracellular potassium concentration, the system will turn to be dominated by two stable equilibrium points. If extracellular potassium concentration is increased more, these two stable equilibrium points will turn back to a single stable equilibrium point again. Hahn and Durand [11] studied a complicated 19-compartment hippocampal pyramidal

* Corresponding author: Tzyy-Leng Horng
Tel: +886-4-24517250 ext. 5126; Fax: +886-4-24510801
E-mail: tlhorng@math.fcu.edu.tw

cell (HPC) model and a reduced two-component HPC model. They found a similar bi-stability featured by the co-existence of a stable equilibrium point and limit cycle, the co-existence of stable repetitive firing and fixed resting states in their phrase, when increasing extracellular potassium concentration. Bi-stability of a stable equilibrium point and limit cycle is of particular interest in forming and annihilation of repetitive neuron firing, which is related to the phenomenon of single-pulse triggering and annihilation [2].

Few investigations were done about bifurcation of permeability of ionic channels in terms of maximum conductance. Schmid et al. [12] studied the blocking effect on ionic channels by reducing the maximum conductance of sodium and potassium channels through a modified stochastic Hodgkin-Huxley model, and found spontaneous oscillation only occurs when the potassium channel is blocked. In the current paper, besides extracellular potassium concentration, we investigate the bifurcations along the maximum conductance of the sodium and potassium channel in the original Hodgkin-Huxley equations without external stimulus, which has never been fully investigated before based on the literatures we have reviewed. Our goal is to find how the permeability of ionic channel would affect the action potential dynamics of a neuron, and focus on spontaneous oscillation. The modulation of permeability of an ionic channel can be simulated by changing its maximum conductance, which can be verified in experiments by adding a channel activator to increase or a blocker to decrease this permeability.

## Mathematical Model and Numerical Method

The popular Hodgkin-Huxley model was originally derived to describe the dynamics of cell membrane action potential of squid axon [1], and has become a basic template for all advanced neuron models thereafter. The equations are

$$\frac{dV}{dt}=\frac{-1}{C_m}(I_{Na}+I_K+I_L)+I_{stim}, \tag{1}$$

where $V$ denotes the trans-membrane action potential; $C_m$ the capacitance and $C_m=1\mu Fcm^{-2}$ usually; $I_{Na}$ the sodium ionic channel current; $I_K$ the potassium ionic channel current; $I_L$ the leakage current (it represents other kinds of ionic channel currents than sodium and potassium); $I_{stim}$ the external stimulus.

The sodium current is further expressed by Ohm's law:

$$I_{Na}=g_{Na}(V-E_{Na})=\bar{g}_{Na}m^3h(V-E_{Na}),$$

where $E_{Na}$ is the sodium reverse potential; $g_{Na}$ the conductance of sodium channel; $\bar{g}_{Na}$ the maximum conductance of sodium channel; $m$ the sodium activation gating variable; $h$ the sodium inactivation gating variable. Usually $E_{Na}=50mV$ and $\bar{g}_{Na}=120ms\cdot cm^{-2}$. Similarly, the potassium current can be expressed as

$$I_K=g_K(V-E_K)=\bar{g}_Kn^4(V-E_K),$$

where $E_K$ is the potassium reverse potential; $g_K$ the conductance of potassium channel; $\bar{g}_K$ the maximum conductance of potassium channel; n the potassium activation gating variable. Usually $E_K=-77mV$ and $\bar{g}_K=36ms\cdot cm^{-2}$. The leakage current is likewise expressed as

$$I_L=g_L(V-E_L),$$

with $g_L=0.3ms\cdot cm^{-2}$ and $E_L=-54.387mV$.

Gating variables *m*, *h*, and *n* denote the opening probability of channel gates of various kinds with the exponent of it showing the number of gates. They can be modeled by chemical reaction

$$C \underset{\beta_s}{\overset{\alpha_s}{\rightleftharpoons}} O,$$

where C is the opening state, and O is the closing state. Then, by law of mass action,

$$\frac{ds}{dt}=\alpha_s(1-s)-\beta_s s=\frac{s_\infty-s}{\tau_s}, \tag{2}$$

with $s\in\{m,h,n\}$. $\alpha_s$ and $\beta_s$ are reaction rate constants which control the transition between the opening and closing of the gate, and they are generally functions of $V$. $s_\infty$ is the steady state solution, and $\tau_s$ is the associated time constant. The relation between $\alpha_s$, $\beta_s$, $s_\infty$ and $\tau_s$ is

$$s_\infty=\frac{\alpha_s}{\alpha_s+\beta_s},\quad \tau_s=\frac{1}{\alpha_s+\beta_s},$$

$s_\infty$ and $\tau_s$, or $\alpha_s$ and $\beta_s$ equivalently, are determined by curve fitting of experimental data. Usually,

$$\alpha_m=\frac{0.1(V+25)}{e^{0.1(V+25)}-1},\ \beta_m=4e^{\frac{V}{18}}, \tag{3}$$

$$\alpha_h=0.07e^{\frac{V}{20}},\quad \beta_h=\frac{1}{e^{0.1(V+30)}+1}, \tag{4}$$

$$\alpha_n=\frac{0.01(V+10)}{e^{0.1(V+10)}-1},\quad \beta_m=0.125e^{\frac{V}{80}}, \tag{5}$$

Normally, the dynamics of (1) and (2) is dominated by a stable equilibrium point representing the resting potential state. When the external impulsive stimulus $I_{stim}$ is employed above a certain threshold, it will go through a large excursion before settling down to the stable equilibrium point, and forms an action potential.

In the current paper, bifurcations along maximum sodium channel conductance $\bar{g}_{Na}$, maximum potassium channel conductance $\bar{g}_K$, and extracellular potassium concentration $[K^+]_o$ without external stimulus current, $I_{stim}=0$, are investigated. Here, we express

$$\bar{g}_{Na}=120(gNafac),\ \bar{g}_k=36(gKfac),$$

and use gNafac and gKfac individually as the bifurcation parameters. As to the bifurcation study of $[K^+]_o$, $[K^+]_o$ needs to be introduced in the reverse potential of potassium ion by Nernst equation:

Table I. Bifurcation points along gNafac

| Bifurcation point between | V (mV) | m | h | n | gNafac |
|---|---|---|---|---|---|
| I and II | -64.013778 | 0.059419 | 0.561265 | 0.332892 | 1.771337 |
| II and III | -62.077378 | 0.074246 | 0.491727 | 0.363255 | 2.603657 |
| III and IV | -56.003212 | 0.142931 | 0.290431 | 0.459771 | 3.086311 |
| IV and V | -53.587703 | 0.181318 | 0.226837 | 0.497324 | 3.081814 |
| V and VI | -38.742787 | 0.533610 | 0.044175 | 0.692139 | 4.487895 |
| VI and VII | -29.292892 | 0.747528 | 0.018045 | 0.776770 | 8.822605 |

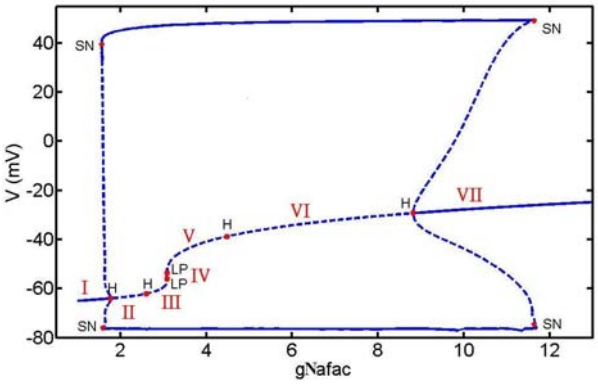


Figure 1. Bifurcation along gNafac projected into *V* vs. gNafac diagram. In equilibria, solid segment represents stable equilibrium points and dashed segment represents unstable ones. In upper and lower limits of limit cycle, solid segment represents stable limit cycles and dashed segment represents unstable ones

$$E_K = \frac{RT}{zF}\ln(\frac{[K^+]_o}{[K^+]_i}),$$

where $[K^+]_i$=400mM, $[K^+]_o$=20mM are the intra-cellular and extracellular potassium concentrations under normal condition; $R$=8.315 J/(mol K) is the gas constant; $T$=310 $K$ is the room temperature in degrees of Kelvin; $z$=1 is the valence of potassium ion; $F$=96485 Coulomb/mol is the Faraday's constant. In the current study, we use XPPAUT [13] to do the numerical bifurcation analysis.

## Results and Discussion

### *3.1 Bifurcation along maximum conductance of sodium channel*

The bifurcation along gNafac projected into *V* vs. gNafac diagram is shown in Figure 1. There are six bifurcation points, shown in Table I, along the equilibria, which separate the equilibria into seven regions marked from I to VII on the diagram. Attractors such as stable equilibrium point, stable limit cycle, and saddle point happening in each region are projected into *V* vs. *m* diagram and shown in Figure 2 respectively. Most of region I has a stable equilibrium point only, which represents the resting potential state. As gNafac is

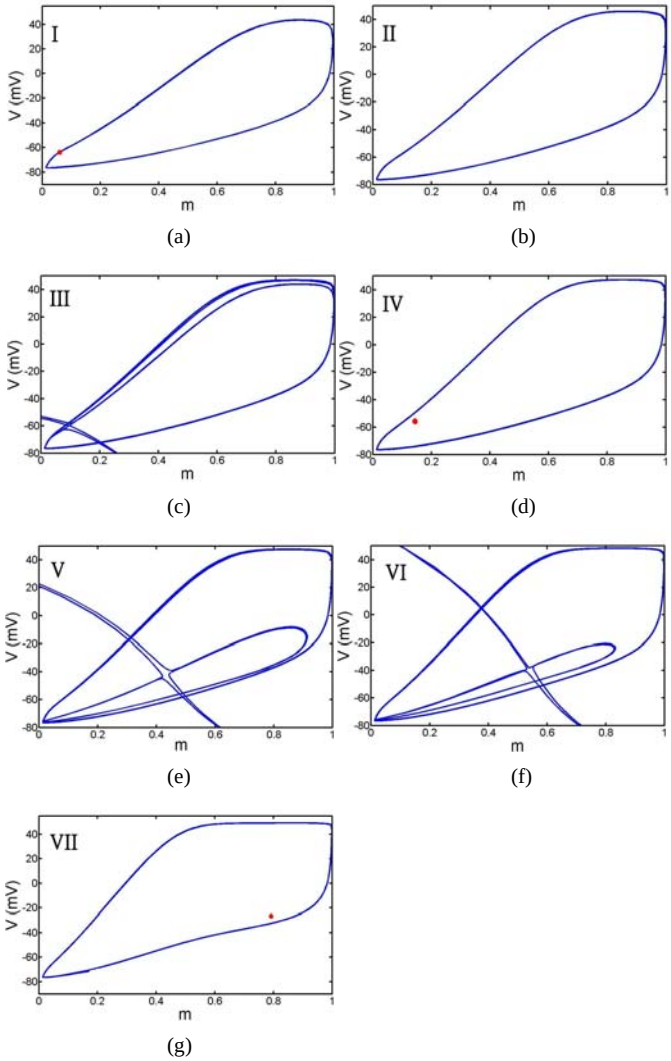


Figure 2. (a) Bi-stability featured by a co-existence of stable limit cycle and equilibrium point in region I with gNafac=1.77. (b) A stable limit cycle in region II with gNafac=2.3.(c) A stable limit cycle and a saddle point in region III with gNafac=2.9. (d) A stable equilibrium point and limit cycle in region IV with gNafac=3.086. (e) A stable limit cycle and a saddle point in region V with gNafac=3.5. (f) A stable limit cycle and a saddle point in region VI with gNafac=5. (g) Bi-stability featured by a co-existence of stable limit cycle and equilibrium point in region VII with gNafac=11

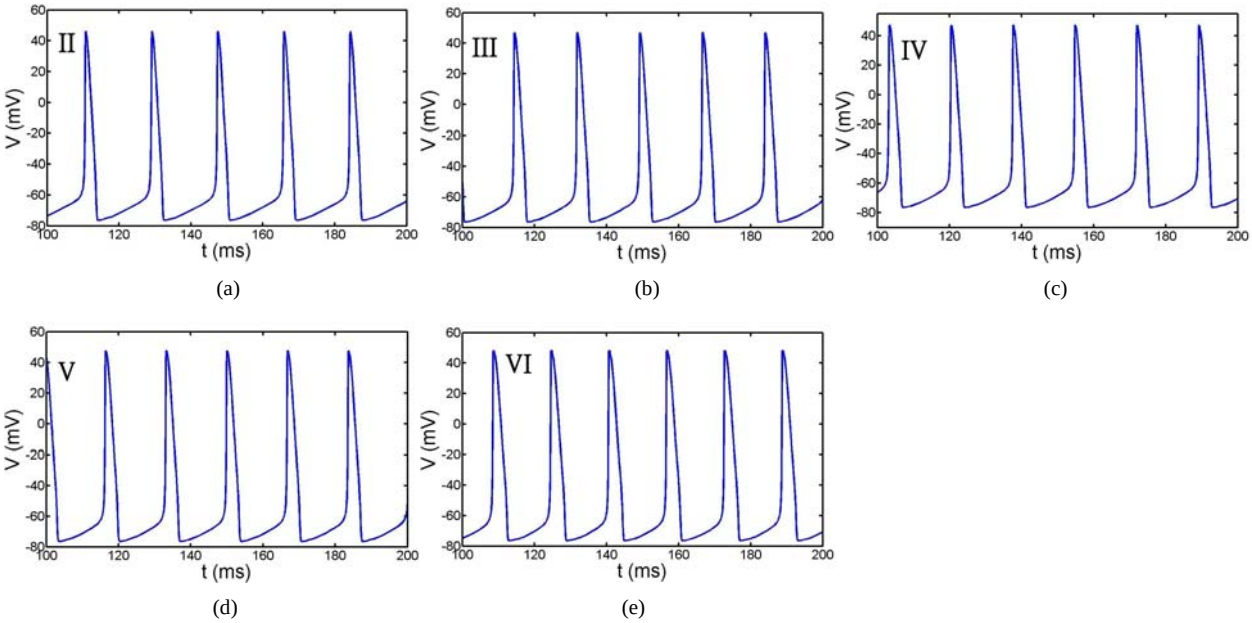


Figure 3. Spontaneous oscillation in region II-VI: (a) in region II with gNafac=2.3, (b) in region III with gNafac=2.9, (c) in region IV with gNafac=3.086, (d) in region V with gNafac=3.5, (e) in region VI with gNafac=5

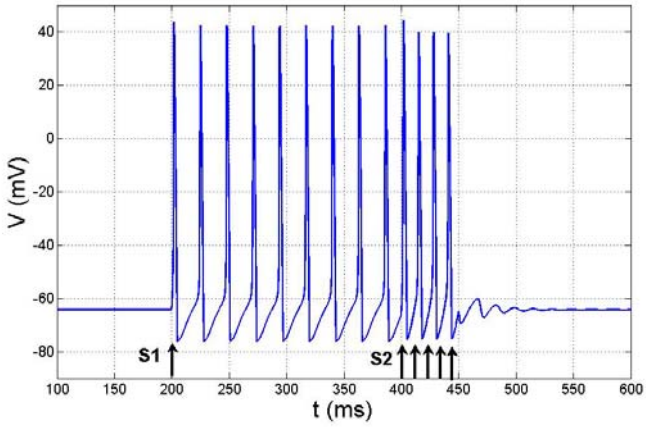


Figure 4. Single-pulse triggering and annihilation in a bi-stable state featuring a co-existence of stable limit cycle and equilibrium point. Here gNafac=1.6, first stimulus current $S1 = 10\mu A/cm^2$ lasts for 1 ms, and the second stimulus current $S2 = 10\mu A/cm^2$ lasts for 50 ms. The spontaneous oscillation (stable limit cycle) is triggered by S1 from the resting potential state (stable equilibrium point) and annihilated later by S2, and the action potential goes back to the resting potential state again

increased towards region II, a saddle-node bifurcation of limit cycles occurs with the emergence of a pair of stable and unstable limit cycles [2], and creates a short interval of bi-stability featured by the coexistence of a stable equilibrium point and limit cycle as shown in Figure 2(a). It looks like the stable equilibrium point is located right on the stable limit cycle as it appears in Figure. 2(a). In fact, the stable equilibrium pint is very near but not on the stable limit cycle. Further increasing gNafac, region I bifurcates to region II, which is a subcritical Hopf bifurcation with the stable equilibrium point in region I becoming unstable in region II, the unstable limit cycle disappearing, and the stable limit cycle remaining. This stable limit cycle remains all the way down to region VI and part of region VII with the upper and lower limits of spontaneous oscillation almost unchanged as shown in Figure 1. Its frequency slightly increases as gNafac increases and this is shown in Figure 3. Further increasing gNafac from region II to III and etc. only changes the property of equilibrium point. It becomes a saddle point in region III; a stable equilibrium point in region IV; a saddle point in region V; a saddle point in region VI with location far different from that of region V. Increasing gNafac from region VI into region VII, another subcritical Hopf bifurcation occurs. Further increasing gNafac in region VII, another saddle-node bifurcation of limit cycles as in region I happens, and the dynamics is dominated by a single stable equilibrium point again. Bi-stabilities happen in region I, IV, and VII. All these bi-stabilities are a co-existence of stable limit cycle and equilibrium point and its associated phenomenon of single-pulse triggering and annihilation is shown in Figure 4.

The physiological reason for forming spontaneous oscillation via increasing maximum conductance of sodium channel is due to the automatic de-polarization in phase 4 of action potential. In a normal situation, the balance of inward sodium, outward potassium, and leaking currents would have the action potential rest to its resting potential state in phase 4, and the action potential would not rise until next external stimulus is applied. Here, since the maximum conductance of sodium channel is increased, the inward sodium current is slightly larger than the outward potassium current in phase 4. This causes a total net inward current of small amount and increases the action potential gradually until it reaches the threshold and rises quickly to form another action potential.

Table II. Bifurcation points along gKfac

| Bifurcation point between | V (mV) | m | h | n | gKfac |
|---|---|---|---|---|---|
| I and II | -62.226498 | 0.072999 | 0.497087 | 0.360899 | 0.549249 |
| II and III | -59.076957 | 0.103551 | 0.386626 | 0.410991 | 0.381637 |
| III and IV | -39.447748 | 0.515186 | 0.047570 | 0.684612 | 0.220006 |
| IV and V | -29.726872 | 0.739503 | 0.018724 | 0.773498 | 0.106770 |

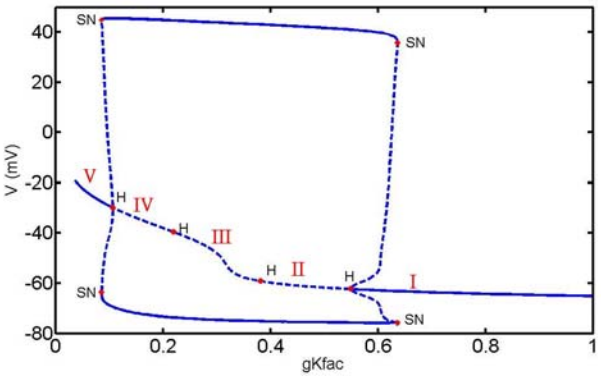


Figure 5. Bifurcation along gKfac projected into *V* vs. gKfac diagram. In equilibria, solid segment represents stable equilibrium points and dashed segment represents unstable ones. In upper and lower limits of limit cycle, solid segment represents stable limit cycles and dashed segment represents unstable ones

### *3.2 Bifurcation along maximum conductance of potassium channel*

The bifurcation along gKfac is similar to gNafac except that bifurcations all happen as gKfac decreases. The bifurcation along gKfac projected into *V* vs. gKfac diagram is shown in Figure 5. It has four bifurcation points, shown in Table II, that separate the equilibria into five regions marked from I to V along the equilibria. Like the case of gNafac, attractors such as stable equilibrium point, stable limit cycle, and saddle point happening in each region are projected into *V* vs. *m* diagram and shown in Figure 6 respectively. Saddle-node bifurcation of limit cycles happens in regions I and V, and subcritical Hopf bifurcation occurs between region I and II, IV and V respectively. The stable limit cycle spans from region I to V with the lower and upper limits of oscillation almost unchanged as shown in Figure 5. The frequency of oscillation slightly increases as gKfac decreases, and this is shown in Figure 7. The stable equilibrium point in region I evolves into an unstable one in region II; a saddle point in region III; another saddle point in region IV that has location far different from that of region III; finally a stable equilibrium point again in region V. Bi-stability occurs at region I and V featuring the co-existence of a stable limit cycle and equilibrium point. It again looks like the stable equilibrium point is located right on the stable limit cycle as it appears in Figure 6(a). In fact, the stable equilibrium point is very near but not right on the stable limit cycle.

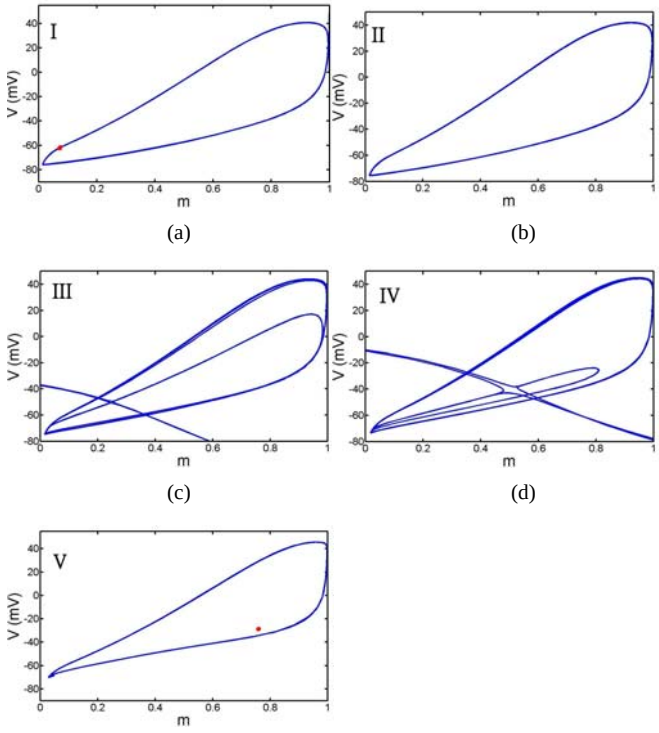


Figure 6. (a) Bi-stability featured by a co-existence of stable limit cycle and equilibrium point in region I with gKfac=0.578. (b) A stable limit cycle in region II with gKfac=0.5.(c) A stable limit cycle and a saddle point in region III with gKfac=0.3. (d) A stable limit cycle and a saddle point in region IV with gKfac=0.2. (e) Bi-stability featured by a co-existence of stable limit cycle and equilibrium point in region V with gKfac=0.09

The physiological reason for forming spontaneous oscillation via decreasing maximum conductance of potassium channel is due to the net inward current of a small amount in phase 4 of action potential the same as the mechanism described in session 3.1. Unlike increasing maximum conductance of sodium channel, this net inward current is due to the decreasing of outward potassium current through the decrease of its maximum conductance.

### *3.3 Bifurcation along extracellular potassium concentration*

The bifurcation along $[K^+]_o$ is much simpler compared with those of gNafac and gKfac. It happens as $[K^+]_o$ increases, and the bifurcation projected into V vs. $[K^+]_o$ diagram is shown in Figure 8. It has only two bifurcation

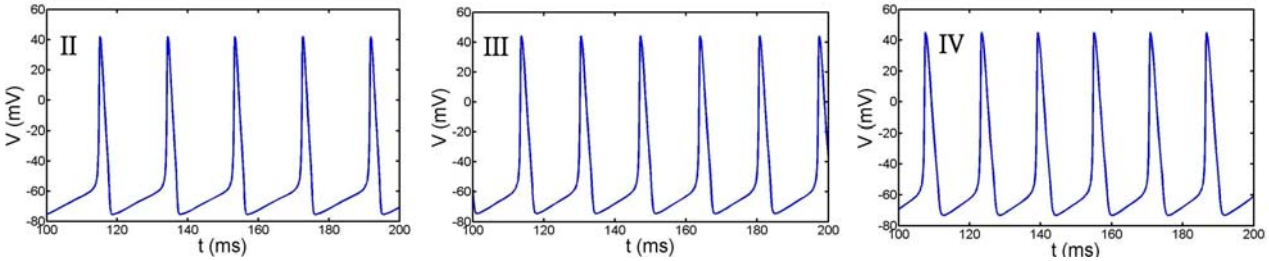


(a) (b) (c)

Figure 7. Spontaneous oscillation in region II-IV: (a) in region II with gKfac=0.5, (b) in region III with gKfac=0.3, (c) in region IV with gKfac=0.2

Table III. Bifurcation points along $[K^+]_o$

| Bifurcation point between | V (mV) | m | h | n | $[K^+]_o$ (mM) |
|---|---|---|---|---|---|
| I and II | -59.913220 | 0.094538 | 0.415147 | 0.397652 | 32.699929 |
| II and III | -41.622034 | 0.457672 | 0.060083 | 0.660268 | 60.818364 |

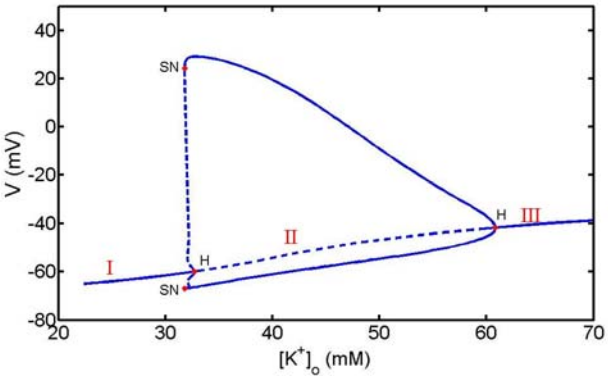


Figure 8. Bifurcation along $[K^+]_o$ projected into *V* vs. $[K^+]_o$ diagram. In equilibria, solid segment represents stable equilibrium points and dashed segment represents unstable ones. In upper and lower limits of limit cycle, solid segment represents stable limit cycles and dashed segment represents unstable ones

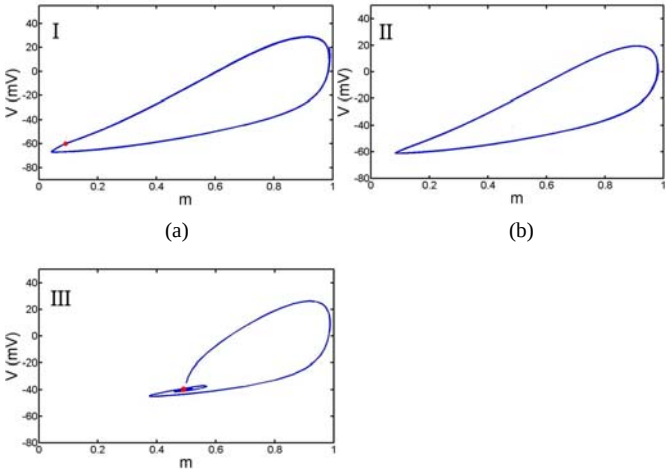


(a) (b) (c)

Figure 9. (a) Bi-stability featured by a co-existence of stable limit cycle and equilibrium point in region I with $[K^+]_o$=32.03 mM. (b) A stable limit cycle in region II with $[K^+]_o$=40 mM. (c) A stable equilibrium point in region III with $[K^+]_o$=65 mM

points, shown in Table III, that separate the equilibria into three regions marked from I to III on the diagram. As above, attractors such as stable equilibrium point, stable limit cycle, and saddle point happening in each region are projected into *V* vs. *m* diagram and shown in Figure 9 respectively. There is a saddle-node bifurcation of limit cycles occurring in region I, followed by a subcritical Hopf bifurcation separating region I and II., and a supercritical Hopf bifurcation separating region II and III. The stable equilibrium point in region I evolves into an unstable one in region II and back to a stable one in region III. The stable limit cycle, mostly residing at region II, has oscillation with amplitude decreasing as $[K^+]_o$ is increased as shown in Figure 8. The frequency of oscillation increases largely as $[K^+]_o$ is increased and this is shown in Figure 10. Bi-stability happens in region I featuring a co-existence of a stable limit cycle and equilibrium point. It again looks like the stable equilibrium point is located right on the stable limit cycle as it appears in Figure 9(a). In fact, the stable equilibrium pint is very near but not right on the stable limit cycle.

The physiological reason of forming spontaneous oscillation via increasing extracellular potassium concentration is also due to the small amount of net inward current in phase 4 of action potential as described above. This net inward current is also due to the decreasing of outward potassium current through the rising of potassium reverse potential $E_K$ by

$$E_K = \frac{RT}{zF}\ln(\frac{[K^+]_o}{[K^+]_i}),$$

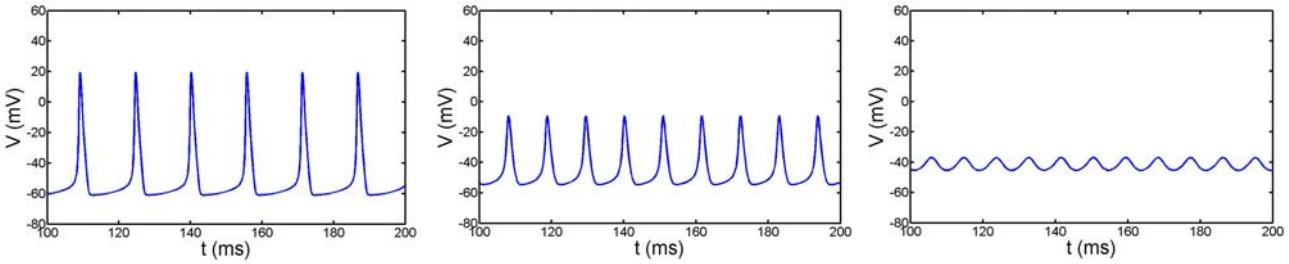


(a) (b) (c)

Figure 10. Spontaneous oscillation in region II: (a) $[K^+]_o$ =40 mM, (b) $[K^+]_o$ =50 mM, (c) $[K^+]_o$ =60 mM

Further increasing extracellular potassium concentration would cause a larger net inward current due to a larger cut in potassium current. This larger net inward current would raise the action potential faster in phase 4 to reach the threshold and form another action potential. This explains why the frequency of oscillation increases as the extracellular potassium concentration is increased as in Figure 10. Since $E_K$ generally serves as the lower bound of the action potential, the increasing of the minimum potential because of increasing the extracellular potassium concentration would make the rise of action potential less in magnitude due to smaller driving force $V - E_{Na}$ . This explains why the oscillation amplitude decreases as the extracellular potassium concentration is increased.

Though the bifurcation along the extracellular sodium concentration is not investigated here, it is expected to have similar dynamics as that of increasing extracellular potassium concentration when the extracellular sodium concentration is increased. That means spontaneous oscillation is expected to happen as the extracellular sodium concentration is increased. We can reason this similarly through the increasing of sodium reverse potential $E_{Na}$ , which serves as the driving force of sodium current. As in session 3.1, it would increase the inward sodium current and make a total net inward current in phase 4 of action potential, which would de-polarize the action potential automatically.

## Conclusion

Our current study via the original Hodgkin-Huxley model shows spontaneous oscillation can be achieved through increasing sodium channel maximum conductance, or decreasing potassium channel maximum conductance, or increasing extracellular potassium concentration without any external stimulus current. This spontaneous oscillation is encountered through subcritical Hopf bifurcation of the resting potential state. It has been observed in experiments that increasing extracellular potassium concentration will indeed cause repetitive neuron firing [11]. We hope our new discovery of causing automatic neuron firing through increasing sodium channel maximum conductance or decreasing potassium channel maximum conductance can also be verified by experiments in the future. As we know, bifurcation analysis is based on the change of model parameters, and changing parameters means extrapolation of the original model which is semi-empirically derived from curve fitting of experimental data under normal situations. We never know if we have over-extrapolated the model in some circumstances so that the original model no longer holds, unless the bifurcation is verified by experiments. We suggest implementing the experiment by the following ways. Increasing sodium channel maximum conductance is equivalent to increase the permeability of sodium channel, which can be done by adding sodium channel activator, usually a neurotransmitter such as acetylcholine (ACh) that binds to acetylcholine receptor and opens a sodium channel. Neurotoxins such as veratridine, scorpion $\alpha$ toxin, and batrachotoxin are also candidates for sodium channel activator [14,15]. Decreasing potassium channel maximum conductance is equivalent to decreasing the permeability of potassium channel, which can be implemented by adding potassium channel inactivator or blocker such as tetraethylammonium (TEA) [16].

## References

[1] A. L. Hodgkin and A. F. Huxley, "A quantitative description of membrane current and its application to conduction and excitation in nerve," *J. Physiol.*, 117:500-544, 1952.

[2] M. R. Guevara, "Bifurcations involving fixed points and limit cycles in biological systems," in A. Beuter, L. Glass, M. C. Mackey, and M. S. Titcombe, Nonlinear Dynamics in Physiology and Medicine. New York: Springer-Verlag, ch.3: 41-85, 2003.

[3] A. Borisyuk and J. Rinzel , "Understanding neuronal dynamics by geometrical dissection of minimal models," in C. Chow, B. Gutkin, D. Hansel, C. Meunier, and J. Dalibard, Models and Methods in Neurophysics, Session LXXX, Lecture Notes of Les Houches Summer School 2003. Elsevier, ch.2:19-72, 2005.

[4] J. Guckenheimer and R. A. Oliva, "Chaos in the Hodgkin–Huxley model," *SIADS*, 1:105-114, 2002.

[5] H. Fukai, T. Nomura, S. Doi, and S. Sato, "Hopf bifurcations in multiple-parameter space of the hodgkin-huxley equations II. Singularity theoretic approach and highly degenerate bifurcations," *Biol. Cybern.*, 82(3):223-9, 2000.

[6] E. M. Izhikevich, "Neural excitability, spiking, and bursting," *Int. J. Bif. Chaos*, 10:1171-1266, 2000.

[7] R. FitzHugh, "Theoretical effect of temperature on threshold in the Hodgkin-Huxley nerve model," *J. Gen. Physiol.*, 49: 989-1005, 1966.

[8] R. S. Guttman and R. Barnhill, "Oscillation and repetitive firing in squid axons," *J. Gen. Physiol.*, 55:104–118, 1970.

[9] U. Feudel, A. Neiman, X. Pei, W. Wojtenek, H. A. Braun, M. T.

Huber, and F. Moss, “Homoclinic bifurcations in a Hodgkin-Huxley model of thermally sensitive neurons,” *Chaos*, 10: 231-239, 2000.

[10] K. Aihara and G. Matsumoto, “Two stable steady states in the Hodgkin-Huxley axon”, *Biophys J*., 41(1): 87–89, 1983.

[11] P. J. Hahn and D. M. Durand , “Bistability dynamics in dimulations of neural activity in high-extracellular-potassium conditions,” *Journal of Computational Neuroscience*, 11:5–18, 2001

[12] G. Schmid, I. Goychuk, and P. Hanggi, “Effect of channel block on the spiking activity of excitable membranes in a stochastic Hodgkin-Huxley model,” *Phys. Biol.*, 1(1-2):61-66, 2004.

[13] B. Ermentrout, Simulating, Analyzing, and Animating Dynamical Systems: A Guide to XPPAUT for Researchers and Students. Philadelphia: SIAM, 2002.

[14] B. Dargent and F. Couraud, “Down-regulation of voltage-dependent sodium channels initiated by sodium influx in developing neurons,” *Proc. Nati. Acad. Sci. USA*, 87:5907-5911, 1990.

[15] A. R. Massensini, M. A. Romano-Silva, and M. V. Gomez, “Sodium channel toxins and neurotransmitter release,” *Neurochemical Research*, 28(10):1607–1611, 2003.

[16] M. J. Lenaeus, M. Vamvouka, P. J. Focia, and A. Gross, **“**Structural basis of TEA blockade in a model potassium channel,” *Nat. Struct. Mol. Biol.*, 12(5):454-9, 2005.